Published OnlineFirst June 30, 2014; DOI: 10.1158/1078-0432.CCR-13-2810

Clinical Cancer Research

Imaging, Diagnosis, Prognosis

Improved Differentiation of Benign and Malignant Breast Tumors with Multiparametric ^{18}Fluorodeoxyglucose Positron Emission Tomography Magnetic Resonance Imaging: A Feasibility Study

Katja Pinker[1], Wolfgang Bogner[2], Pascal Baltzer[1], Georgios Karanikas[3], Heinrich Magometschnigg[1], Peter Brader[1], Stephan Gruber[2], Hubert Bickel[1], Peter Dubsky[4], Zsuzsanna Bago-Horvath[5], Rupert Bartsch[6], Michael Weber[3], Siegfried Trattnig[2], and Thomas H. Helbich[1]

Abstract

Purpose: To assess whether multiparametric ^{18}fluorodeoxyglucose positron emission tomography magnetic resonance imaging (MRI) (MP ^{18}FDG PET-MRI) using dynamic contrast-enhanced MRI (DCE-MRI), diffusion-weighted imaging (DWI), three-dimensional proton MR spectroscopic imaging (3D ^{1}H-MRSI), and ^{18}FDG-PET enables an improved differentiation of benign and malignant breast tumors.

Experimental Design: Seventy-six female patients (mean age, 55.7 years; range, 25–86 years) with an imaging abnormality (BI-RADS 0, 4–5) were included in this Institutional Review Board (IRB)-approved study. Patients underwent fused PET-MRI of the breast with ^{18}FDG-PET/CT and MP MRI at 3T. The likelihood of malignancy was assessed for all single parameters, for MP MRI with two/three parameters, and for MP ^{18}FDG PET-MRI. Histopathology was used as the standard of reference. Appropriate statistical tests were used to assess sensitivity, specificity, and diagnostic accuracy for each assessment combination.

Results: There were 53 malignant and 23 benign breast lesions. MP ^{18}FDG PET-MRI yielded a significantly higher area under the cure (AUC) of 0.935 than DCE-MRI (AUC, 0.86; $P = 0.044$) and the combination of DCE-MRI and another parameter (AUC, 0.761–0.826; $P = 0.013$–0.020). MP ^{18}FDG PET-MRI showed slight further improvement to MP MRI with three parameters (AUC, 0.925; $P = 0.317$). Using MP ^{18}FDG PET-MRI there would have been a reduction of the unnecessary breast biopsies recommended by MP imaging with one or two parameters ($P = 0.002$–0.011).

Conclusion: This feasibility study shows that MP ^{18}FDG PET-MRI enables an improved differentiation of benign and malignant breast tumors when several MRI and PET parameters are combined. MP ^{18}FDG PET-MRI may lead to a reduction in unnecessary breast biopsies. *Clin Cancer Res; 20(13); 3540–9. ©2014 AACR.*

Introduction

In the last several years, multiparametric (MP) MRI and positron emission tomography (PET) of the breast have emerged as promising imaging tools (1–4). MP MRI provides morphologic and functional information that results in a high sensitivity and improved specificity (5–8). ^{18}Fluorodeoxyglucose (^{18}FDG)-PET provides functional data on tumor metabolism and has been found to be of complementary value (9, 10). To overcome the limitations of morphologic and functional imaging techniques, hybrid imaging systems have been developed and introduced into the clinical routine (11, 12). Better imaging techniques for breast cancer could result in more accurate tumor detection and staging, leading to further improvement in outcomes for patients, and thus, the combined use of MP PET-MRI has widespread applications.

Essentially, 3 different fields of applications are feasible with MP ^{18}FDG PET-MRI: (i) morphologic information can be merged with functional information; (ii) functional imaging parameters can be monitored; and (iii) molecular and metabolic processes involved in cancer development can be observed at different levels. To date, the potential of MP PET-MRI in the assessment of breast tumors has not been explored in detail.

Authors' Affiliations: [1]Department of Biomedical Imaging and Image-guided Therapy, Division of Molecular and Gender Imaging, [2]Department of Biomedical Imaging and Image-guided Therapy, MR Centre of Excellence, [3]Department of Biomedical Imaging and Image-guided Therapy, Division of Nuclear Medicine, Departments of [4]Surgery and [5]Pathology, and [6]Department of Internal Medicine, Division of Oncology, Medical University of Vienna, Vienna, Austria

Note: Supplementary data for this article are available at Clinical Cancer Research Online (http://clincancerres.aacrjournals.org/).

Corresponding Author: Thomas H. Helbich, Department of Biomedical Imaging and Image-guided Therapy, Division of Molecular and Gender Imaging, Medical University of Vienna, Waehringer Guertel 18–20, Vienna, 1090 Austria. Phone: 431404004820; Fax: 431404004898; E-mail: thomas.helbich@meduniwien.ac.at

doi: 10.1158/1078-0432.CCR-13-2810

Published OnlineFirst June 30, 2014; DOI: 10.1158/1078-0432.CCR-13-2810

Translational Relevance

We hypothesized that through the noninvasive quantitative assessment of multiple processes (tumor neoangiogenesis, microstructural changes, increased glucose consumption, and cell membrane turnover) involved in cancer growth, an improved differentiation of breast tumors would be possible with multiparametric (MP) ^{18}fluorodeoxyglucose positron emission tomography MRI (^{18}FDG PET-MRI), using dynamic contrast-enhanced (DCE)-MRI, diffusion-weighted imaging (DWI), three-dimensional proton MR spectroscopic imaging (3D ^{1}H-MRSI), and ^{18}FDG-PET. This feasibility study shows that MP ^{18}FDG PET-MRI allows an improved differentiation of benign and malignant breast tumors by assessing multiple processes involved in cancer development combining several MRI and PET parameters. In addition, MP ^{18}FDG PET-MRI may lead to a reduction in unnecessary breast biopsies. To our knowledge, this is the first study that has performed MP ^{18}FDG PET-MRI for the assessment of breast tumors in a clinical setting. The data suggest that MP ^{18}FDG PET-MRI may have widespread applications in the diagnosis, staging, and assessment of the treatment response in breast cancer.

We hypothesized that through the noninvasive quantitative assessment of multiple processes (tumor neoangiogenesis, microstructural changes, increased glucose consumption, and cell membrane turnover) involved in cancer growth (13), an improved differentiation of benign and malignant breast tumors would be provided by MP ^{18}FDG PET-MRI. Thus, the aim of our study was to assess whether MP ^{18}FDG PET-MRI enables an improved differentiation of benign and malignant breast tumors. To reach this goal, we used the currently available MP MRI parameters [dynamic contrast-enhanced MRI (DCE-MRI), diffusion-weighted imaging (DWI), and 3-dimensional proton MR spectroscopic imaging (3D ^{1}H-MRSI)] and the combination of these with the radiotracer ^{18}FDG for the assessment of tissue metabolism with PET.

Materials and Methods

Patients

From January 2010 to December 2012, 76 consecutive patients (mean age, 55.7 years; range, 25–86 years) were included in this Institutional Review Board (IRB)-approved, prospective, single-institution study. All patients fulfilled the following inclusion criteria and underwent MP ^{18}FDG PET-MRI: 18 years or older; not pregnant; not breastfeeding; suspicious finding at mammography or breast ultrasonography (US), i.e., asymmetric density, architectural distortion, breast mass, or microcalcifications (BI-RADS 0, further imaging warranted; 4, suspicious abnormality; 5, highly suggestive for malignancy); no previous treatment; and no contraindications for MRI or MRI contrast agents (2). Twenty-five patients presented with clinical symptoms and were referred for further work-up. Fifty-one patients were asymptomatic, had a screen-detected imaging abnormality, and were referred for assessment. Written informed consent was obtained from all patients before MP ^{18}FDG PET-MRI. Regardless of the results of MP ^{18}FDG PET-MRI, histopathologic verification was performed of the tumor in question. Histopathologic verification was always performed after MP ^{18}FDG PET-MRI.

The initial BI-RADS category distributions of study lesions before MP ^{18}FDG PET-MRI were: BI-RADS 0 for 9 lesions, BI-RADS 4 for 24 lesions, and BI-RADS 5 for 43 lesions.

Imaging

All patients underwent MP ^{18}FDG PET-MRI with PET/computed tomography (CT) using ^{18}FDG and MP MRI of the breast at 3T. Examinations were scheduled no longer than 7 days apart (mean, 1.9; range 0–7; same day, $n = 29$; 1 day, $n = 16$; 2 days, $n = 6$; 3 days, $n = 8$; 4 days, $n = 5$; 5 days, $n = 2$; 6 days, $n = 2$; 7 days, $n = 8$). PET and MRI images were fused semiautomatically to generate MP ^{18}FDG PET-MRI data.

^{18}FDG-PET/CT. All imaging studies were performed using a combined PET/CT in-line system (Biograph 64 TruePoint PET/CT system, Siemens). Patients fasted 5 hours before body weight–adapted injection of approximately 200 to 350 MBq ^{18}FDG. Scanning started 45 minutes after injection. Blood glucose levels were <150 mg/dL (8.3 mmol/L). A prone PET dataset of the breasts and a low-dose unenhanced CT scan for attenuation correction were recorded. PET images were reconstructed using the iterative TrueX algorithm (Siemens), which incorporates a specific correction for the point-spread function in addition to commonly used correction factors (14, 15). Four iterations per 21 subsets were used, with a matrix size of 168 × 168, a trans-axial field of view of 605 mm (pixel size, 3.6 mm), and a section thickness of 5 mm. Further technical details are provided by the manufacturer (16). For each patient, ^{18}FDG-PET and MR images were transferred to a TrueD fusion workstation (Siemens). The DCE-MRI dataset was treated as the reference volume, and the ^{18}FDG-PET dataset was treated as the volume to be registered. Both datasets were fused semiautomatically by using the "landmark matching" tool of the TrueD workstation and color-coded images were generated.

MP MRI. All imaging studies were performed with the patient in the prone position using a 3T MRI (Tim Trio, Siemens) and a four-channel breast coil (InVivo). In premenopausal women, MRI was performed in the second week of the menstrual cycle to minimize breast parenchymal enhancement. The MRI protocol consisted of:

1. An axial T_2-weighted turbo spin echo sequence with fat-saturation [time to repetition (TR)/echo time (TE)/inversion time (TI), 4,800/61/230 ms; field of view (FOV), 340 mm; 34 slices at 4 mm; matrix, 314 × 320; one average; acquisition time (TA), 2:26 minutes)].

Published OnlineFirst June 30, 2014; DOI: 10.1158/1078-0432.CCR-13-2810

2. An axial diffusion-weighted, double-refocused, single-shot echo-planar imaging sequence with inversion recovery fat suppression [TR/TE/TI: 13,700/83/220 ms; FOV, 340 × 117 mm^2; 40 slices at 3.5 mm; matrix, 192 × 64 (50% oversampling); 2 averages; *b* values, 50 and 850 s/mm^2; TA, 3:19 minutes; ref. 17].
3. A point-resolved spectroscopic sequence (PRESS) with spectral water and fat suppression and spatial outer volume suppression (TR/TE: 750/145 ms; FOV, 12 × 12 × 12 cm^3; matrix, 12 × 12 × 12; 5 averages; TA, 11:17 minutes). Three-dimensional (3D) ^{1}H-MRSI was acquired before DCE-MRI to avoid any influence of the contrast agent on the detected Choline (Cho) signal (18).
4. A split dynamics DCE-MRI protocol combining high-spatial and high-temporal resolution with the following parameters: T_1-weighted volume-interpolated breathhold examination (VIBE) sequences (TR/TE: 3.61/1.4 ms; FOVr, 320 mm; 72 slices; 1.7 mm isotropic; matrix, 192 × 192; one average; 13.2 seconds per volume) with a total TA of 15:20 minutes and T_1-weighted turbo fast-low-angle shot (FLASH) 3D sequences with selective water excitation (TR/TE: 877/3.82 ms; FOV, 320 mm; 96 slices; 1 mm isotropic; matrix, 320 × 134; one average; 2 minutes; ref. 19).

Gadoteratemeglumine (Gd-DOTA; Dotarem) was injected intravenously as a bolus (0.1 mmol/kg body weight) using a power injector (Spectris Solaris EP, Medrad) at 4 m:/s followed by a 20 mL saline flush. The total MRI examination time was about 34 minutes.

Data analysis

An experienced breast radiologist (K. Pinker, 7 years of experience) and a nuclear medicine physician (G. Karanikas, >20 years of experience) prospectively evaluated the MP ^{18}FDG PET-MRI data. MP ^{18}FDG PET-MRI datasets were assessed according to the following criteria. Both readers, in consensus, determined the probability of malignancy for MP ^{18}FDG PET-MRI data as previous studies have shown very good intra- and interobserver agreement by using the following evaluation of each imaging parameter (17, 20). The readers were aware that the patients had a breast tumor, but they were provided with neither the previous mammographic and sonographic imaging data nor the histopathologic results.

Single parameters. *DCE-MRI.* DCE-MRI imaging data were assessed for lesion type [mass or non-mass enhancement (NME)], lesion morphology, and enhancement kinetics using the descriptors defined in the American College of Radiology (ACR) MRI BI-RADS lexicon. For the assessment of the enhancement kinetics of masses, an automated semiquantitative curve type analysis was performed using a dedicated software (Syngo BreVis, Siemens). For NME, the enhancement kinetics were not considered (8, 19, 21, 22). The probability of malignancy was determined by assigning a final BI-RADS category as summarized in Supplementary Table S2 (8). Lesion size was recorded measuring the largest diameter of the tumor in the axial plane.

DWI. High *b* value DW images (i.e., 850 s/mm^2) were visually assessed for hyperintense areas corresponding to the contrast-enhancing tumor on DC-MRI. Three-dimensional regions of interest (ROI) were drawn manually on apparent diffusion coefficient (ADC) maps for all contrast-enhancing tumors, and the mean ADC was determined and used for differentiation between benign and malignant lesions. Bogner and colleagues evaluated the diagnostic quality of DWI with regard to ADC accuracy at 3T. On the basis of ROC curves, the optimal ADC threshold of 1.25 × 10^{-3} mm^2/s for the differentiation of benign and malignant lesions breast lesions at 3T was determined (17). This ADC threshold was applied in the current study. Lesions were classified as benign if ADC values were equal to or above and malignant if below 1.25 × 10^{-3} mm^2/s.

3D ^{1}H-MRSI. An experienced spectroscopist (S. Gruber, >10 years of experience) evaluated all 3D ^{1}H-MRSI data.

All 3D ^{1}H-MRSI voxels in the tumor volume, which was detected with DCE-MRI, were evaluated for elevated levels of Cho at the chemical shift of 3.23 ppm, and the voxel with the maximum Cho signal-to-noise ratio (SNR) was determined by measuring the ratio between the Cho peak and the baseline noise amplitude at >7 ppm. Gruber and colleagues evaluated the diagnostic accuracy of 3D ^{1}H-MRSI for the differentiation of benign and malignant breast lesions at 3T, on the basis of Cho SNR threshold levels (18). It was demonstrated that a Cho SNR threshold level of 2.6 at 3T provided the best sensitivity and specificity. This Cho SNR threshold level was applied in the current study. Lesions were classified as malignant if SNR was equal to or greater than 2.6 and benign if SNR was lower than 2.6.

^{18}FDG-PET. All ^{18}FDG-PET images were evaluated for an increased tracer uptake. Semiquantitative analysis was performed using body weight–corrected standard uptake values (SUV). Maximum SUVs were calculated using ROIs (9 × 9 pixel) chosen over all areas of abnormal ^{18}FDG uptake. When no increased ^{18}FDG uptake was seen or no tumor was seen on CT or on PET images, the ROIs were placed in the region of the tumor indicated by DCE-MRI. Previous studies have demonstrated that the use of a maximum SUV threshold for differentiation between benign and malignant breast lesions is not reliable (23, 24). Thus, the maximum SUV values were obtained but not used as strict threshold values for malignancy. To differentiate between benign and malignant lesions, tumors within tissues of mild metabolic activity were classified as positive for malignancy when ^{18}FDG uptake was greater than blood pool activity. Tumors within tissues demonstrating moderate or high physiologic activity were considered positive for malignancy if the activity was greater than the adjacent physiologic activity (9, 25).

Two parameters. Imaging with DCE-MRI and one additional functional parameter (DWI, 3D ^{1}H-MRSI, or ^{18}FDG-PET) was classified as positive if at least one imaging parameter was indicative of malignancy.

Published OnlineFirst June 30, 2014; DOI: 10.1158/1078-0432.CCR-13-2810

MP MRI with three parameters. For assessment of MP MRI using DCE-MRI, DWI, and 3D ^{1}H-MRSI, the following reading scheme was used:

1. If DCE-MRI, DWI, and ^{1}H-MRSI of the breast were positive, MP MRI was considered positive for malignancy.
2. If DCE-MRI, DWI, and ^{1}H-MRSI of the breast were negative, MP MRI was considered negative for malignancy.
3. If 2 of the 3 parameters were positive, MP MRI was considered positive for malignancy. If 2 of the 3 parameters were negative, MP MRI was considered negative for malignancy.

MP ^{18}FDG PET-MRI with four parameters. For assessment of MP ^{18}FDG PET-MRI, the following reading scheme was used:

1. If all 4 parameters were indicative of malignancy, MP ^{18}FDG PET-MRI was considered positive (Supplementary Figs. S1 and S2).
2. If all 4 parameters were indicative of benignity, MP ^{18}FDG PET-MRI was classified as negative.
3. If 3 of 4 parameters were indicative of malignancy, MP ^{18}FDG PET-MRI was classified as positive (Figs. 1 and 2).
4. If 3 of 4 parameters were indicative of benignity, MP ^{18}FDG PET-MRI was classified as negative (Figs. 3 and 4).
5. In case of a tie where 2 parameters were positive and 2 negative, MP ^{18}FDG PET-MRI was considered positive if DCE-MRI was indicative of malignancy and negative if DCE-MRI was indicative of benignity.

Histopathology

The final diagnosis was established by histopathology, by an experienced pathologist (Z. Bago-Horvath, >6 years of experience in breast pathology), obtained with either image-guided needle biopsy (26) or surgery. In case of a benign diagnosis on image-guided needle biopsy, the final diagnosis was considered benign ($n = 21$). In case of a high-risk lesion on biopsy, the final diagnosis was established with surgery ($n = 2$; ref. 27). Lesions considered as high-risk were atypical ductal hyperplasia, atypical lobular hyperplasia, atypical columnar cell hyperplasia, lobular carcinoma *in situ*, papillary lesions of the breast, flat epithelial atypia, or radial scar/complex sclerosing lesions. All malignant lesions were scheduled for surgery after image-guided needle biopsy ($n = 53$). Needle biopsy was performed by either ultrasound guidance ($n = 69$) or stereotactic X-ray guidance ($n = 7$) using either 14G core needle biopsy or 9G vacuum-assisted core needle biopsy.

Statistical analysis

Statistical analysis was performed by a statistician using SPSS 19.0 (CIA version 2.2.0). All calculations were performed on a per-lesion basis. Sensitivity, specificity, accuracy, negative predictive value (NPV), positive predictive

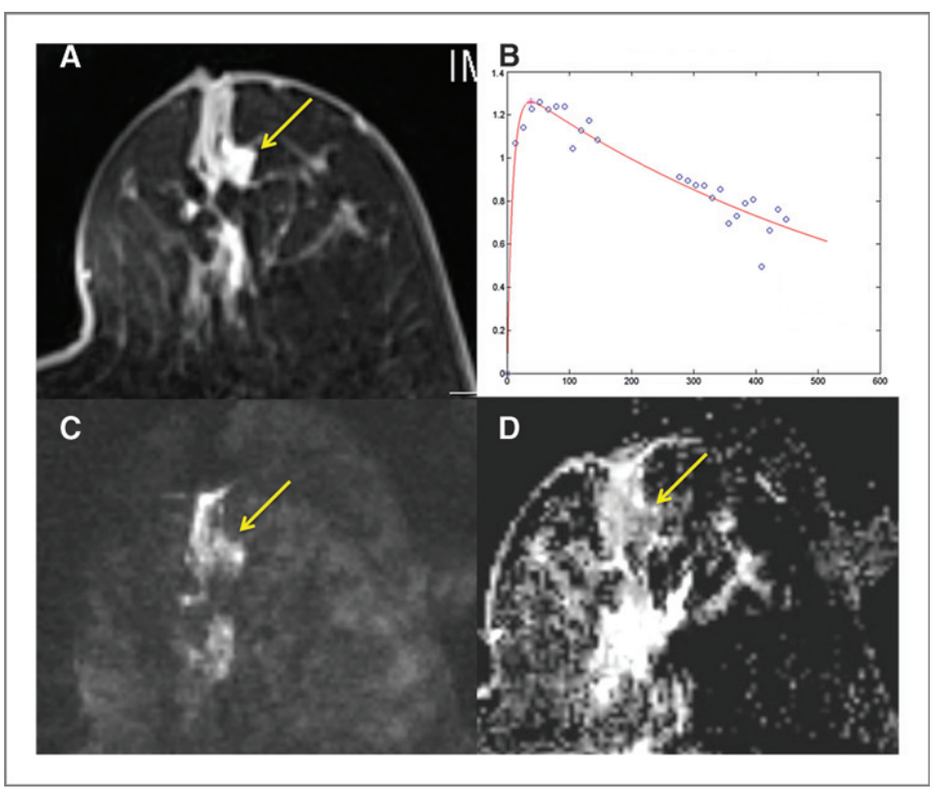

Figure 1. Invasive ductal carcinoma G3 in a 63-year-old woman, laterally in the left breast retroareolar. A, arrow, the indistinct irregular mass lesion shows (B) a heterogeneous initial strong enhancement followed by a washout and was classified by DCE-MRI of the breast as BI-RADS 5 (highly suggestive for malignancy). C, on DWI, the mass lesion is bright and (D) demonstrates decreased ADC values (0.82×10^{-3} mm^2/s) and is, therefore, considered malignant.

Published OnlineFirst June 30, 2014; DOI: 10.1158/1078-0432.CCR-13-2810

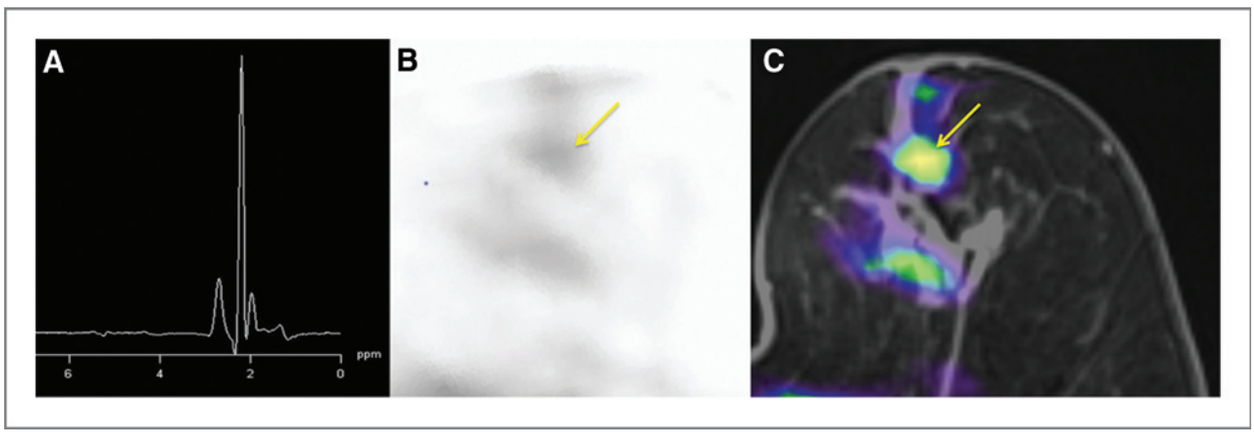

Figure 2. Invasive ductal carcinoma G3 in a 63-year-old woman, laterally in the left breast retroareolar (continued from Fig. 1). A, on 3D ^{1}H-MRSI, the lesion is false-negative, as there were no elevated Cho levels. B, on ^{18}FDG-PET, the lesion is moderately ^{18}FDG-avid, with a maximum SUV of 2.08. C, according to the evaluation algorithm, an accurate classification as malignant with MP ^{18}FDG PET-MRI was possible because 3 of the parameters were considered positive.

value (PPV), and their 95% confidence intervals (CI) were calculated for MP ^{18}FDG PET-MRI, MP MRI, and DCE-MRI and one additional functional parameter (DWI, 3D ^{1}H-MRSI, ^{18}FDG-PET/CT) and all single parameters. Histopathology was used as the gold standard. Significant differences in sensitivity, specificity, and accuracy were assessed with generalized estimation equations (GEE) and *post hoc* simple contrast tests were performed. Because of the small number of benign lesions, no multiplicity corrections were performed to avoid an increasing error of the second type. ROC curves were plotted and the AUC was determined. Statistical differences between the AUCs were assessed using the method proposed by DeLong and colleagues (28). $P \leq 0.05$ was considered a significant result.

Results

A total of 76 tumors were detected, ranging from 5 to 77 mm (mean, 29.2 mm; median, 24 mm; interquartile range, 24 mm). Histopathology classified 53 tumors as malignant and 23 tumors as benign.

Detailed results of DCE-MRI of the breast, DWI, 3D ^{1}H-MRSI, and ^{18}FDG-PET, the assigned final MRI BI-RADS classification and histopathology are provided in Supplementary Table S1.

There were 67 enhancing masses and 9 NME lesions on DCE-MRI of the breast. BI-RADS diagnosis, quantitative curve types, ADC, Cho SNR, and maximum SUV results stratified by final histopathologic diagnosis are summarized in Table 1.

Sensitivities, specificities, diagnostic accuracies, and the AUCs for the assessment of a single parameter, MP MRI with combinations of 2/3 parameters, and MP ^{18}FDG PET-MRI with 4 parameters are summarized in Table 2.

MP ^{18}FDG PET-MRI achieved the highest sensitivity, with 100%, and an improved specificity of 87%, resulting in the highest diagnostic accuracy of 96%, with an AUC of 0.935. None of the assessments with a single parameter (AUC, 0.829–0.94) or 2 parameters (AUC, 0.761–0.826) or 3 parameters (AUC, 0.925) achieved results as good as that. Assessment with the single-parameter DWI and 3D ^{1}H-MRSI allowed an increase in specificity up to 96%. However, there was a reduction in sensitivity ranging from 83% to 96%. Although assessment with 2 parameters maximized sensitivity, there was a trade-off in specificity, which ranged from 52% to 65%.

The ROC analysis of MP ^{18}FDG PET-MRI showed a clear improvement in the differentiation of benign and malignant breast lesions compared with all parameters and their combinations (Supplementary Fig. S3). This difference was significant for the most commonly used technique for breast MRI, namely DCE-MRI, and the combination of DCE-MRI and another parameter. There was no significant difference for the single-parameter DWI and 3D ^{1}H-MRSI. These results have limited value because neither DWI nor 3D ^{1}H-MRSI can be used for diagnosis without the information provided by DCE-MRI. MP ^{18}FDG PET-MRI showed a slight further improvement compared with MP MRI with 3 parameters.

Detailed histopathologic results for all false-positive and false-negative lesions for MP ^{18}FDG PET-MRI, MP MRI, DCE-MRI with one additional functional parameter, and all single parameters are provided in Supplementary Table S3.

Using MP ^{18}FDG PET-MRI, there would have been a reduction of unnecessary breast biopsies recommended by DCE-MRI alone (50%, 3 of 6) and the combination of DCE-MRI and another parameter ($\leq$38%, 3 of 8–10). Because of the small sample size, this reduction was borderline significant for DCE-MRI ($P = 0.063$) but significant for the combination of DCE-MRI and another parameter ($P = 0.002$–0.011).

Discussion

The results of our study show that MP ^{18}FDG PET-MRI allows an improved differentiation of benign and malignant breast tumors compared with the most commonly used MRI

Published OnlineFirst June 30, 2014; DOI: 10.1158/1078-0432.CCR-13-2810

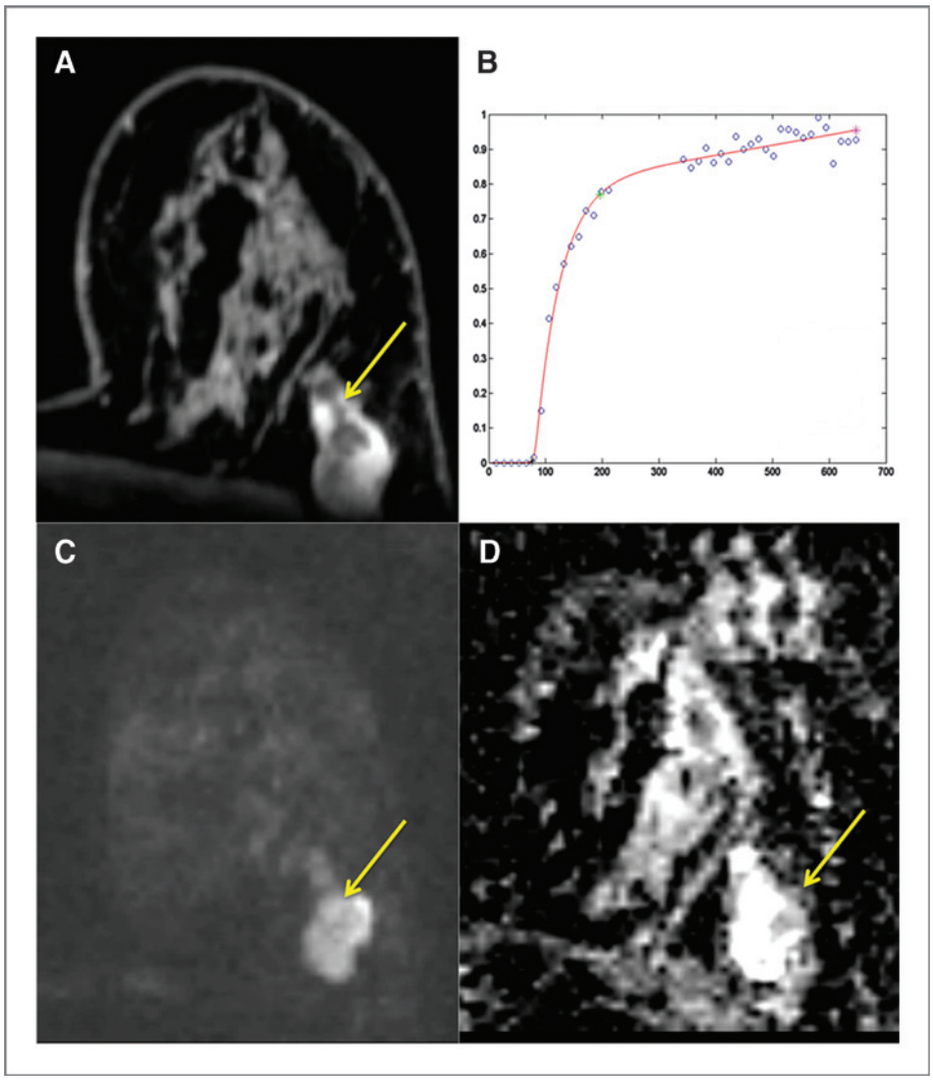

Figure 3. Fibroadenoma in a 40-year-old woman, laterally in the left breast. A, arrow, the lobulated mass with nonenhancing septa shows (B) a persistent homogeneous internal enhancement and was classified by DCE-MRI of the breast as BI-RADS 2 (benign). C, on DWI, the mass lesion is bright due to a "T2-shine-through" and (D) has no decreased ADC values (1.55×10^{-3} mm^2/s).

and PET parameters that use 1 parameter or a combination of up to 3 parameters. The effectiveness of MP ^{18}FDG PET-MRI is reflected by the highest diagnostic accuracy for breast cancer diagnosis, resulting in a significantly improved AUC. In addition, in this study, MP ^{18}FDG PET-MRI led to a reduction in unnecessary breast biopsies. MP ^{18}FDG PET-MRI enables the acquisition of a multitude of imaging parameters (DCE-MRI, DWI, 3D ^{1}H-MRSI, ^{18}FDG-PET) and each of these parameters has an incremental value. DCE-MRI of the breast provides high-resolution anatomic information and enables the depiction of increased microvascular density and capillary leaks in malignant breast tumors as a marker of neoangiogenesis (29). DWI depicts cellular diffusivity, which is typically restricted in malignant tissue (7, 20). 3D ^{1}H-MRSI detects elevated levels of the metabolite choline as a marker of an increased cell membrane turnover (6). ^{18}FDG-PET allows an assessment of glucose consumption, which is typically increased in neoplastic processes (3, 30). By combining the information from all these parameters, MP ^{18}FDG PET-MRI provides an improved differentiation of benign and malignant breast tumors.

Compared with MP MRI, which combines 3 parameters (DCE, DWI, 3D ^{1}H-MRSI), MP ^{18}FDG PET-MRI added slightly more information about the differentiation of benign and malignant breast lesions by correctly diagnosing an NME as malignant, which would have been deemed benign on MP MRI with 3 parameters due to negative DWI and 3D ^{1}H-MRSI. The additional information provided by the fourth parameter is not as great as anticipated. This is due to the fact that MP MRI with 3 parameters has a high diagnostic accuracy and ^{18}FDG, the tracer used in this study has a good sensitivity, but limited specificity. Several types of benign breast diseases can be ^{18}FDG-avid and mimic malignancy (3). Several new radiotracers that are designed to visualize the processes involved in cancer formation and progression are currently being translated from experimental to clinical imaging, such as ^{18}F-fluorodeoxythymidine (^{18}FLT) and ^{18}F-deoxyfluoroarabinofuranosylthymine

Published OnlineFirst June 30, 2014; DOI: 10.1158/1078-0432.CCR-13-2810

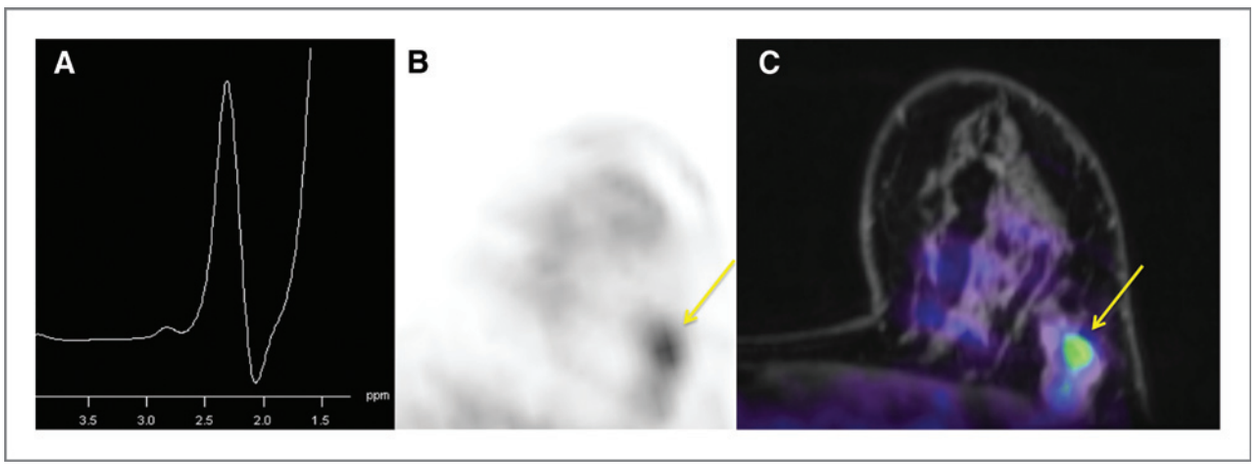

Figure 4. Fibroadenoma in a 40-year-old woman, laterally in the left breast (continued from Fig. 3). A, there are no elevated Cho levels on 3D ^{1}H-MRSI (SNR < 2.5). B, on ^{18}FDG-PET, the lesion is moderately ^{18}FDG-avid, with a maximum SUV of 2.73. The lesion was false-positive on PET but true-negative on DCE-MRI, DWI, and 3D ^{1}H-MRSI. C, according to the evaluation algorithm, the tumor was accurately classified as benign by MP ^{18}FDG PET-MRI.

(^{18}FMAU) for DNA synthesis and cell proliferation; ^{18}F-fluoromisonidazole (^{1}FMISO) for the assessment of tumor hypoxia, which is associated with metastatic potential; or ^{18}F-fluoroestradiol (^{18}FES) for the assessment of receptor status (31). With the use of more specific radiotracers, hardware and software improvements, MP PET-MRI has the potential to become a very important tool in breast imaging by displaying the hallmarks of cancer.

With MP PET-MRI, using the radiotracer ^{18}FDG, there were 3 false-positives. One false-positive lesion was a high-risk lesion, which was a lesion with atypia at surgery. High-risk lesions are defined as lesions with an uncertain potential for malignancy (27, 32), and the suspicious features at MP ^{18}FDG PET-MRI probably reflect this potential or an imminent malignant transformation. The other 2 false-positives were clinically asymptomatic chronic abscesses. These lesions were suspicious on DCE-MRI, demonstrated low ADC values on DWI (33), and were ^{18}FDG-avid, compatible with abscess and inflammation mimicking malignancy (3). Only 3D ^{1}H-MRSI was correctly negative.

MP MRI is defined as the combination of DCE MRI with one or more MRI parameters, such as DWI or 3D ^{1}H-MRSI. Several studies have investigated MP MRI with the combination of 2 parameters (DCE-MRI and DWI or DCE-MRI and ^{1}H-MRSI) and reported encouraging results with an increase in specificity (34–37). In all these studies, the improvement in specificity led to a trade-off in sensitivity.

In contrast, the combination approach of 2 parameters in this study led to an increase in sensitivity to 100% but no increase in specificity. The combination approach even decreased specificity and AUC compared with single parametric imaging. This was due to the fact that with the chosen combination approach, MP MRI with 2 parameters was considered positive if one parameter was indicative of malignancy. This highlights the challenges of combining MP data in clinical practice. Initial results of MP MRI with 3 parameters demonstrated a further increase in diagnostic accuracy compared with various combinations of 2 parameters (38). A further improvement in the differentiation of benign and malignant breast lesions with MP MRI can be expected by the addition or replacement of new and more sensitive parameters, such as sodium imaging (39), chemical exchange saturation transfer (CEST) imaging (40), or hyperpolarized MRSI (41). This also highlights the potential of supplemental information provided by ^{18}FDG-PET with hybrid imaging systems (42, 43).

In this study, we evaluated several single parameters. Single parametric imaging with DCE-MRI is the mainstay of breast MRI, with an excellent sensitivity but limited

Table 1. BI-RADS diagnosis, quantitative curve types, ADC, Cho SNR and maximum SUV results stratified by final histopathological diagnosis for all breast tumors

	BI-RADS 2/3	BI-RADS 4/5	Type 1 curve	Type 2 curve	Type 3 curve	ADC[a]	SNR[a]	SUV_{max}
Benign	17 (73.9)	6 (26.1)	8 (42.1)	5 (26.3)	6 (31.6)	1.551, 0.259	0, 1.4	2.4, 1.5
Malignant	1 (1.9)	52 (98.1)	3 (6.3)	5 (10.4)	40 (83.3)	0.900, 0.320	5.9, 8.9	6.2, 5.6

NOTE: If not specified otherwise, values are given in numbers and percentages in parentheses.

Abbreviation: SUV_{max}, maximum standard uptake values.

[a]Values are given as median, interquartile range.

Published OnlineFirst June 30, 2014; DOI: 10.1158/1078-0432.CCR-13-2810

Table 2. Sensitivities, specificities, diagnostic accuracy, AUC, and 95% CIs (in parentheses) for the assessment of a single parameter, MP MRI with combinations of 2/3 parameters, and MP^{18}FDG PET-MRI with 4 parameters

	Sensitivity	Specificity	Accuracy	AUC	*P*
Single parameter					
DCE-MRI	98% (90%–99%)	74% (56%–92%)	91% (84%–97%)	0.86 (0.798–0.972)[a]	**0.044**
DWI	96% (87%–99%)	96% (87%–99%)	92% (86%–98%)	0.894 (0.798–0.991)	0.110
3D ^{1}H-MRSI	83% (71%–91%)	91% (80–100%)	86% (78%–93%)	0.872 (0.782–0.962)	0.172
^{18}FDG-PET	96% (87%–99%)	70% (51%–88%)	88% (81%–95%)	0.829 (0.710–0.948)[a]	**0.020**
DCE-MRI and DWI	100% (93%100%)	65% (44%–81%)	89% (83%–96%)	0.826 (0.7030–0.949)[a]	**0.013**
Two parameters					
DCE-MRI and 3D ^{1}H-MRSI	100% (93%–100%)	61% (41%–78%)	88% (81%–95%)	0.804 (0.676–0.933)[a]	**0.013**
DCE-MRI and ^{18}FDG-PET	100% (93%–100%)	52% (33%–71%)	86% (78%–93%)	0.761 (0.624–0.897)[a]	**0.001**
MP MRI					
DCE-MRI, DWI, and 3D ^{1}H-MRSI	98% (93%–100%)	87% (73%–100%)	95% (90%–100%)	0.925 (0.841–1)	0.317
MP ^{18}FDG PET-MRI					
DCE-MRI, DWI, 3D 1H-MRSI, ^{18}FDG-PET	100% (90%–100%)	87% (73%–100%)	96% (90%–100%)	0.935 (0.835–1)	—

[a]Significantly different from MP ^{18}FDG PET-MRI ($P < 0.05$).

specificity. It has been demonstrated that even with the use of high-field scanners and parallel imaging, there are limits to what is achievable with DCE-MRI (1, 8, 19, 42, 44). Other single parameters included DWI and 3D ^{1}H-MRSI. In this study, these parameters had higher specificities, but, for this increase in specificity, there was a trade-off in sensitivity. In addition, neither DWI nor 3D ^{1}H-MRSI are standalone parameters and cannot be used for diagnosis without the information provided by DCE-MRI (18, 22). ^{18}FDG-PET has a sensitivity comparable to DWI and 3D ^{1}H-MRSI and, similar to DCE-MRI, is limited in specificity (3). Thus, ^{18}FDG-PET is currently not considered as a diagnostic tool in breast imaging, although a study using dedicated systems showed promising results (45).

The current study has some limitations. One limitation is that the distribution of benign and malignant tumors, as well as histopathologic subtypes, is not well balanced. This has relevant implications for specificity. Although there were significant differences in the AUC for MP ^{18}FDG PET-MRI, compared with all other parameters except DWI, 3D ^{1}H-MRSI, and MP MRI with 3 parameters, the differences about specificity and diagnostic accuracy were not significant as the corresponding tests were underpowered because of low sample size. This study aimed to prove the feasibility of our diagnostic approach for MP ^{18}FDG PET-MRI. The classification system used in our study is based on empirical clinical experience and applies single-parameter thresholds based on previously published data (8, 17–19, 22, 46). The study design did not aim to validate acknowledged thresholds or develop a classification model based on multivariate statistics or machine learning methods. These methods need large databases, which have not been published as yet (47). However, MP ^{18}FDG PET-MRI is increasingly used in clinical practice. This underlines the necessity of a simple reading scheme that can be used in clinical practice. Such a reading scheme is currently not available and was prospectively tested in our study. The anticipated increase in specificity and diagnostic accuracy should be addressed in prospective studies with larger patient numbers. In the current study, the median tumor size was 24 mm. Therefore, the results of this study might not be equally applicable to smaller tumors and need to be tested in future studies. Using MP ^{18}FDG PET-MRI, there would have been a reduction of unnecessary breast biopsies recommended by DCE-MRI or MP with 2 parameters alone in 50% of cases. However, this theoretical reduction in unnecessary biopsies is hampered by the small sample size and should be further addressed in larger studies. In this study, not all patients underwent MP ^{18}FDG PET-MRI on the same day (mean, 1.9; range, 0–7). However, this delay between examinations was short, with a maximum range of 7 days, and relevant changes in the tumor microenvironment in this time span were not expected. Another limitation is that all patients underwent fused but not simultaneous MP ^{18}FDG PET-MRI. Simultaneous PET-MRI scanners are now becoming clinically available (48), and it can be expected that the proposed reading scheme for MP ^{18}FDG PET-MRI in breast tumors will be equally applicable to simultaneous MP ^{18}FDG PET-MRI. All MR examinations were performed at 3T rather than 1.5T, which is the most commonly used field strength in breast MRI. As all commercially available synchronous PET-MRI scanners operate at a field strength of 3T to exploit the inherent benefit of a higher SNR, which can be translated into a higher resolution or a deeper insight into tumor biology, this cannot be seen as a limitation.

In conclusion, this feasibility study shows that MP ^{18}FDG PET-MRI enables an improved differentiation of benign and malignant breast tumors by assessing the multiple processes

Published OnlineFirst June 30, 2014; DOI: 10.1158/1078-0432.CCR-13-2810

involved in cancer development through the combination of several MRI and PET parameters. In addition, MP ^{18}FDG PET-MRI may lead to a reduction in unnecessary breast biopsies. The data suggest that MP ^{18}FDG PET-MRI may have widespread applications, not only in the diagnosis and staging of breast of cancer but also for the assessment of treatment response.

Disclosure of Potential Conflicts of Interest

No potential conflicts of interest were disclosed.

Authors' Contributions

Conception and design: K. Pinker, P. Baltzer, G. Karanikas, P. Brader, S. Gruber, S. Trattnig, T.H. Helbich

Development of methodology: K. Pinker, W. Bogner, P. Brader, S. Trattnig, T.H. Helbich

Acquisition of data (provided animals, acquired and managed patients, provided facilities, etc.): K. Pinker, W. Bogner, P. Baltzer, H. Magometschnigg, P. Brader, S. Gruber, H. Bickel, P. Dubsky, Z. Bago-Horvath, R. Bartsch, T.H. Helbich

Analysis and interpretation of data (e.g., statistical analysis, biostatistics, computational analysis): K. Pinker, P. Baltzer, H. Magometschnigg, S. Gruber, P. Dubsky, Z. Bago-Horvath, M. Weber

Writing, review, and or revision of the manuscript: K. Pinker, W. Bogner, P. Baltzer, P. Brader, S. Gruber, H. Bickel, P. Dubsky, Z. Bago-Horvath, R. Bartsch, M. Weber, S. Trattnig, T.H. Helbich

Administrative, technical, or material support (i.e., reporting or organizing data, constructing databases): K. Pinker, H. Magometschnigg, S. Trattnig

Study supervision: K. Pinker, P. Brader, S. Trattnig, T.H. Helbich

Grant Support

The funding was provided by the Austrian Society of Senology Scientific Funding Award 2009, the Austrian Nationalbank "Jubiläumsfond" Project Nr. 13652, and the Medical Scientific Fund of the Mayor of Vienna Project No. 10029.

The costs of publication of this article were defrayed in part by the payment of page charges. This article must therefore be hereby marked *advertisement* in accordance with 18 U.S.C. Section 1734 solely to indicate this fact.

Received October 19, 2013; revised March 14, 2014; accepted April 7, 2014; published OnlineFirst June 24, 2014.

References

1. Morris EA. Diagnostic breast MR imaging: current status and future directions. Radiol Clin North Am 2007;45:863–80.
2. Sardanelli F, Boetes C, Borisch B, Decker T, Federico M, Gilbert FJ, et al. Magnetic resonance imaging of the breast: recommendations from the EUSOMA working group. Eur J Cancer 2010;46:1296–316.
3. Avril N, Adler LP. F-18 fluorodeoxyglucose-positron emission tomography imaging for primary breast cancer and loco-regional staging. Radiol Clin North Am 2007;45:645–57.
4. Zytoon AA, Murakami K, El-Kholy MR, El-Shorbagy E. Dual time point FDG-PET/CT imaging. . . Potential tool for diagnosis of breast cancer. Clin Radiol 2008;63:1213–27.
5. Birdwell RL, Mountford CE, Iglehart JD. Molecular imaging of the breast. Radiol Clin North Am 2010;48:1075–88.
6. Baltzer PA, Dietzel M. Breast lesions: diagnosis by using proton MR spectroscopy at 1.5 and 3.0 T–systematic review and meta-analysis. Radiology 2013;267:735–46.
7. Chen X, Li WL, Zhang YL, Wu Q, Guo YM, Bai ZL. Meta-analysis of quantitative diffusion-weighted MR imaging in the differential diagnosis of breast lesions. BMC Cancer 2010;10:693.
8. Pinker-Domenig K, Bogner W, Gruber S, Bickel H, Duffy S, Schernthaner M, et al. High resolution MRI of the breast at 3 T: which BI-RADS(R) descriptors are most strongly associated with the diagnosis of breast cancer? Eur Radiol 2012;22:322–30.
9. Moy L, Ponzo F, Noz ME, Maguire GQ, Murphy-Walcott AD, Deans AE, et al. Improving specificity of breast MRI using prone PET and fused MRI and PET 3D volume datasets. Eur J Nucl Med 2007;48:528–37.
10. Kumar R, Lal N, Alavi A. 18F-FDG PET in detecting primary breast cancer. Eur J Nucl Med 2007;48:1751; author reply 1752.
11. Wehrl HF, Judenhofer MS, Wiehr S, Pichler BJ. Pre-clinical PET/MR: technological advances and new perspectives in biomedical research. Eur J Nucl Med Mol Imaging 2009;36 Suppl 1:S56–68.
12. Judenhofer MS, Wehrl HF, Newport DF, Catana C, Siegel SB, Becker M, et al. Simultaneous PET-MRI: a new approach for functional and morphological imaging. Nat Med 2008;14:459–65.
13. Hanahan D, Weinberg RA. The hallmarks of cancer. Cell 2000;100:57–70.
14. Knausl B, Hirtl A, Dobrozemsky G, Bergmann H, Kletter K, Dudczak R, et al. PET based volume segmentation with emphasis on the iterative TrueX algorithm. Z Med Phys 2012;22:29–39.
15. Rapisarda E, Bettinardi V, Thielemans K, Gilardi MC. Image-based point spread function implementation in a fully 3D OSEM reconstruction algorithm for PET. Phys Med Biol 2010;55:4131–51.
16. Solutions SM. Biograph True Point PET-CT: system specifications; 2007 [cited 2012 May 21]; Available from: http://www.medical.siemens.com/siemens/en_GB/gg_nm_FBAs/files/brochures/Biograph/Biograph_spec_sheet_0507.pdf.
17. Bogner W, Gruber S, Pinker K, Grabner G, Stadlbauer A, Weber M, et al. Diffusion-weighted MR for differentiation of breast lesions at 3.0 T: how does selection of diffusion protocols affect diagnosis? Radiology 2009;253:341–51.
18. Gruber S, Debski BK, Pinker K, Chmelik M, Grabner G, Helbich T, et al. Three-dimensional proton MR spectroscopic imaging at 3 T for the differentiation of benign and malignant breast lesions. Radiology 2011;261:752–61.
19. Pinker K, Grabner G, Bogner W, Gruber S, Szomolanyi P, Trattnig S, et al. A combined high temporal and high spatial resolution 3 Tesla MR imaging protocol for the assessment of breast lesions: initial results. Invest Radiol 2009;44:553–8.
20. Bogner W, Pinker-Domenig K, Bickel H, Chmelik M, Weber M, Helbich TH, et al. Readout-segmented echo-planar imaging improves the diagnostic performance of diffusion-weighted MR breast examinations at 3.0 T. Radiology 2012;263:64–76.
21. Kuhl CK, Schild HH, Morakkabati N. Dynamic bilateral contrast-enhanced MR imaging of the breast: trade-off between spatial and temporal resolution. Radiology 2005;236:789–800.
22. Pinker K, Bickel H, Helbich T, Gruber S, Dubsky P, Pluschnig U, et al. Combined contrast enhanced magnetic resonance and diffusion weighted imaging reading adapted to the "Breast Imaging Reporting and Data System" for multiparametric 3 T imaging of breast lesions. Eur Radiol 2013;23:1791–802.
23. Kumar R, Chauhan A, Zhuang H, Chandra P, Schnall M, Alavi A. Standardized uptake values of normal breast tissue with 2-deoxy-2-[F-18]fluoro-D: -glucose positron emission tomography: variations with age, breast density, and menopausal status. Mol Imaging Biol 2006;8:355–62.
24. Zytoon AA, Murakami K, El-Kholy MR, El-Shorbagy E, Ebied O. Breast cancer with low FDG uptake: characterization by means of dual-time point FDG-PET/CT. Eur J Radiol 2009;70:530–8.
25. Moy L, Noz ME, Maguire GQ Jr, Ponzo F, Deans AE, Murphy-Walcott AD, et al. Prone mammoPET acquisition improves the ability to fuse MRI and PET breast scans. Clin Nucl Med 2007;32:194–8.
26. Wallis M, Tardivon A, Helbich T, Schreer I. Guidelines from the European Society of Breast Imaging for diagnostic interventional breast procedures. Eur Radiol 2007;17:581–8.
27. Degnim AC, King TA. Surgical management of high-risk breast lesions. Surg Clin North Am 2013;93:329–40.
28. DeLong ER, DeLong DM, Clarke-Pearson DL. Comparing the areas under two or more correlated receiver operating characteristic curves: a nonparametric approach. Biometrics 1988;44:837–45.

Published OnlineFirst June 30, 2014; DOI: 10.1158/1078-0432.CCR-13-2810

29. Helbich TH, Roberts TP, Gossmann A, Wendland MF, Shames DM, Adachi M, et al. Quantitative gadopentetate-enhanced MRI of breast tumors: testing of different analytic methods. Magn Reson Med 2000;44:915–24.
30. Quon A, Gambhir SS. FDG-PET and beyond: molecular breast cancer imaging. J Clin Oncol 2005;23:1664–73.
31. Dunphy MP, Lewis JS. Radiopharmaceuticals in preclinical and clinical development for monitoring of therapy with PET. J Nucl Med 2009;50 Suppl 1:106S-21S.
32. Riedl CC, Ponhold L, Flory D, Weber M, Kroiss R, Wagner T, et al. Magnetic resonance imaging of the breast improves detection of invasive cancer, preinvasive cancer, and premalignant lesions during surveillance of women at high risk for breast cancer. Clin Cancer Res 2007;13:6144–52.
33. Unal O, Koparan HI, Avcu S, Kalender AM, Kisli E. The diagnostic value of diffusion-weighted magnetic resonance imaging in soft tissue abscesses. Eur J Radiol 2011;77:490–4.
34. Bartella L, Morris EA, Dershaw DD, Liberman L, Thakur SB, Moskowitz C, et al. Proton MR spectroscopy with choline peak as malignancy marker improves positive predictive value for breast cancer diagnosis: preliminary study. Radiology 2006;239:686–92.
35. Ei Khouli RH, Jacobs MA, Mezban SD, Huang P, Kamel IR, Macura KJ, et al. Diffusion-weighted imaging improves the diagnostic accuracy of conventional 3.0-T breast MR imaging. Radiology 2010;256:64–73.
36. Kul S, Cansu A, Alhan E, Dinc H, Gunes G, Reis A. Contribution of diffusion-weighted imaging to dynamic contrast-enhanced MRI in the characterization of breast tumors. Am J Roentgenol 2011;196:210–7.
37. Yabuuchi H, Matsuo Y, Okafuji T, Kamitani T, Soeda H, Setoguchi T, et al. Enhanced mass on contrast-enhanced breast MR imaging: lesion characterization using combination of dynamic contrast-enhanced and diffusion-weighted MR images. J Magn Reson Imaging 2008;28: 1157–65.
38. Pinker K, Bogner W, Baltzer P, Gruber S, Bickel H, Brueck B, et al. Improved diagnostic accuracy with multiparametric magnetic resonance imaging of the breast using dynamic contrast-enhanced MRI, diffusion-weighted imaging and 3D proton MR spectroscopic imaging. Invest Radiol. 2014 Feb 21. [Epub ahead of print].
39. Madelin G, Regatte RR. Biomedical applications of sodium MRI *in vivo*. J Magn Reson Imaging 2013;38:511–29.
40. Schmitt B, Trattnig S, Schlemmer HP. CEST-imaging: a new contrast in MR-mammography by means of chemical exchange saturation transfer. Eur J Radiol 2012;81 Suppl 1:S144–6.
41. Kurhanewicz J, Vigneron DB, Brindle K, Chekmenev EY, Comment A, Cunningham CH, et al. Analysis of cancer metabolism by imaging hyperpolarized nuclei: prospects for translation to clinical research. Neoplasia 2011;13:81–97.
42. Moy L, Mercado CLBreast MRI. In: Magnetic resonance imaging clinics of North America; 2010. Available from: http://www.mri.theclinics.com/.
43. Domingues RC, Carneiro MP, Lopes FC, Domingues RC, da Fonseca LM, Gasparetto EL. Whole-body MRI and FDG PET fused images for evaluation of patients with cancer. Am J Roentgenol 2009;192: 1012–20.
44. Turnbull LW. Dynamic contrast-enhanced MRI in the diagnosis and management of breast cancer. NMR Biomed 2009;22:28–39.
45. Berg WA, Weinberg IN, Narayanan D, Lobrano ME, Ross E, Amodei L, et al. High-resolution fluorodeoxyglucose positron emission tomography with compression ("positron emission mammography") is highly accurate in depicting primary breast cancer. Breast J 2006;12: 309–23.
46. Magometschnigg H, Pinker K, Bickel H, Brueck B, Wengert G, Helbich TH. Dedicated breast PET-CT for the assessment of breast tumors: an alternative for patients unsuitable for CE-MRI? Chicago, IL: Radiology Society of North America; 2012.
47. Bland M. An Introduction to medical statistics. 3rd ed. Oxford Medical Publications; Oxford, UK; 2000.
48. Yankeelov TE, Peterson TE, Abramson RG, Garcia-Izquierdo D, Arlinghaus LR, Li X, et al. Simultaneous PET-MRI in oncology: a solution looking for a problem? Magn Reson Imaging 2012;30: 1342–56.

Published OnlineFirst June 30, 2014; DOI: 10.1158/1078-0432.CCR-13-2810

Clinical Cancer Research

Improved Differentiation of Benign and Malignant Breast Tumors with Multiparametric ^{18}Fluorodeoxyglucose Positron Emission Tomography Magnetic Resonance Imaging: A Feasibility Study

Katja Pinker, Wolfgang Bogner, Pascal Baltzer, et al.

Clin Cancer Res 2014;20:3540-3549. Published OnlineFirst June 30, 2014.